Food Chemistry 368 (2022) 130813

Contents lists available at ScienceDirect

Food Chemistry

journal homepage: www.elsevier.com/locate/foodchem

Development of a PCL-PEO double network colorimetric pH sensor using electrospun fibers containing *Hibiscus rosa sinensis* extract and silver nanoparticles for food monitoring

Lavernchy Jovanska [a,b], Chun-Hui Chiu [c,d], Yi-Cheun Yeh [e], Wen-Dee Chiang [f], Chang-Chi Hsieh [a], Reuben Wang [g,h,*]

[a] Department of Animal Science and Biotechnology, Tunghai University, No. 1727, Sec. 4 Taiwan Boulevard, Xitun District, Taichung 40704, Taiwan
[b] Department of Food Technology, Faculty of Agricultural Technology, Soegijapranata Catholic University, Semarang, Indonesia
[c] Graduate Institute of Health Industry and Technology, Research Center for Chinese Herbal Medicine and Research Center for Food and Cosmetic Safety, College of Human Ecology, Chang Gung University of Science and Technology, Taoyuan City, Taiwan
[d] Department of Traditional Chinese Medicine, Chang Gung Memorial Hospital, Keelung City, Taiwan
[e] Institute of Polymer Science and Engineering, National Taiwan University, Taipei City, Taiwan
[f] Department of Food Science, Tunghai University, Taichung, Taiwan
[g] Master of Public Health Program, College of Public Health, National Taiwan University, Taipei City, Taiwan
[h] Institute of Food Safety and Health, College of Public Health, National Taiwan University, Taipei City, Taiwan

ARTICLE INFO

Keywords:
Anthocyanin
Hibiscus rosa sinensis
Electrospinning
pH sensor
Quality monitoring
Kinetic modeling
Refrigerated fresh foods
Food packaging

ABSTRACT

Major anthocyanin, cyanidin-3-sophoroside (318.1 mg/mL), and other minor copigments were identified in the ethanol extract of *Hibiscus rosa sinensis*. The extracts can be coelectrospun with polycaprolactone and polyethylene oxide into fiber mats and were sensitive to pH changes from 1 to 13 with a unique color code ($\Delta E > 5$). The pH sensor was used to monitor shrimp quality under isothermal conditions to obtain the respective activation energy (Ea in kJ/mol) of the sensors' color-change response (20.2), measured pH (20.6), and trimethylamine nitrogen (24.6), indole (27.1), and total microbial counts (30.8). Together with the Pearson correlation coefficient, the results showed high correlations between the sensors' color change and other quality parameters ($p < 0.001$). The regression equation developed by conducting the kinetic analysis was also suitable for predicting shrimp quality at refrigeration temperatures (4–10 °C) and can be used as a marker to monitor shrimp quality by visually inspecting the item condition.

1. Introduction

Fresh goods are nutrient-dense products of perishable nature. Customers mainly depend on sensory characteristics to determine product freshness, but judgment could be affected if the product has outer shells, such as crustaceans. Previous studies reported that pathogens tend to stay attached to shrimp surfaces despite disinfection, acid or heat treatments. While the mechanisms have yet to be completely understood, porous surfaces such as chitin were found to play a part in shielding pathogens from sanitation treatments, effectively influencing shelf life (Wan Norhana, Poole, Deeth, & Dykes, 2010). The postmortem metabolism of shrimp also makes them more susceptible to postharvest losses than fish. Shrimps have a higher number of enzyme groups that degrade ATP, and faster conversion from ATP to hypoxanthine than fish and shellfishes, along with two paths involved in ATP degradation (Kato, Kunimoto, Koseki, Kitakami, & Arai, 2009). The quality of shrimp is also affected by different postharvest storage and slaughtering treatments. Moreover, there is a possibility of mixing different batches of products together, as the visual difference is not significant. Overall, shrimp are more susceptible to degradation, yet it is harder to determine the difference in freshness (Rahman et al., 2021), making shrimp an interesting model for a quality monitoring sensor. Traditional microbiological and physicochemical analyses have pointed out the important parameters concerning shrimp freshness in order of importance, which are total microbial count (TMC), total volatile basic nitrogen (TVB-N), trimethylamine nitrogen (TMA-N), pH, thiobarbituric acid reactive substances (TBARS) and free fatty acids (FFAs) (Khodanazary, 2019). As an important parameter itself, pH also reflected changes in other

* Corresponding author at: Institute of Food Safety and Health, College of Public Health, National Taiwan University, Taipei City 100025, Taiwan.
E-mail address: reubenwang@ntu.edu.tw (R. Wang).

https://doi.org/10.1016/j.foodchem.2021.130813
Received 18 May 2021; Received in revised form 31 July 2021; Accepted 5 August 2021
Available online 9 August 2021

parameters. For example, lactic acid formation from microbial activity and volatile base nitrogen formation can also alter pH, making it an important marker for freshness monitoring (Kato et al., 2009).

An ideal freshness indicator for shrimp should be simple, quick, easy to visualize, and noninvasive yet accurately reflect the internal condition as opposed to the shell surface condition. Previous studies developed for real-time and *in situ* pH monitoring mostly relied on electrochemical reactions. However, the need to set up electrodes, computing systems or other hardware prevented these methods from being implemented at a larger scale. The materials might also be expensive and unsuitable for commercial application across different types of foodstuffs (Mustapha, Khairuddin, Muhamad, Hashim, & Siddique, 2016). Another way to forego electrochemical reaction analysis is to utilize pH-sensitive compounds. The compounds were immobilized on films and allowed to react with the environment inside food packaging to reflect the freshness of the product. This concept tends to be less expensive, simpler and thus more suitable for commercial application at points of sale. In this format, we have now seen several pH indicators developed for real-time food acidity inspection purposes, among which some of them were made from pigments of natural resources. These pigments, which change colors according to different pH levels, include those from red cabbage (Weston, Phan, Arcot, & Chandrawati, 2020), microalgae (Kuntzler, Costa, Brizio, & Morais, 2020), the fruit of palm trees (Silva, Mastrantonio, Costa, & Morais, 2019), and gromwell roots (Ezati, Bang, & Rhim, 2021).

Although natural dyes are safer for consumption than synthetic dyes when used in direct contact with food, most natural dyes have problems when applying them to pH sensors for food monitoring. First, the colors of most natural dyes developed under a specific range of pH conditions are too similar to differentiate, which is an obstacle for further applications in food monitoring (Ezati, Tajik, & Moradi, 2019). Second, these naturally derived substances are sensitive to light exposure, temperature variations, oxidation, or other adverse environmental conditions during food storage (Devarayan & Kim, 2015). Third, if pH indicators are made from biodegradable materials and do not have antimicrobial activities, microbes may propagate directly on these pH indicators. The formation of biofilm due to microbial growth may block the indicators from direct contact with the food, which results in misinterpretation of pH levels, as the indicator only responds to the pH condition of a certain area containing the growing microbes and not responding to the pH condition of the entire food item.

Previously, natural pigments, including those from açaí (Silva et al., 2019), black carrot (Moradi, Tajik, Almasi, Forough, & Ezati, 2019), and red cabbage (Pourjavaher, Almasi, Meshkini, Pirsa, & Parandi, 2017), had been coelectrospun into fibers to make pH sensors. Although some of the instability issues of pigments were solved after immobilization, commonly shared problems still exist for these sensors, including the leakage of pigments from fibers during pH monitoring, limiting their usage in food monitoring. This is especially true when the robustness of the fibers was highly considered once they were fabricated at the nanoscale and were intended to be used repeatedly during food monitoring. Therefore, it is necessary to know the conditions and methods to address the problems mentioned above, find universal natural dyes that develop differentiable colors under different pH conditions and fabricate them into sensors with favorable properties, which are all essential criteria for effective pH indicators used in food monitoring.

The anthocyanin extract from Shoeblackplant (*Hibiscus rosa sinensis*, HRSE) was chosen as a natural pigment in this study for pH sensing because of its low toxicity and was used as a food ingredient (Burton-Freeman, Sandhu, & Edirisinghe, 2016). The anthocyanins in the pigment extract were quantitatively and qualitatively analyzed by ultra-performance liquid chromatography-tandem mass spectrometry (UPLC-MS/MS) to ensure their consistency in different batches of pigment extraction. In addition, polymer choice and their molecular interactions with pigments were studied carefully by testing polymers in several mixing ratios to minimize pigment leakage. These include the characterization of color accuracy, fiber stability, and reusability of the fabricated sensor before applying it for food monitoring. Finally, this work also aimed to investigate the applicability of the developed pH sensor to monitor the quality of shrimp stored under isothermal conditions. Therefore, the kinetics of shrimp deterioration markers, including TMA-N, indole, pH, and total bacterial count, were examined in parallel with the color change of the colorimetric pH sensor prototype.

2. Materials and methods

2.1. Materials

Polycaprolactone (PCL) (Mw 80,000), polyethylene oxide (PEO) (Mw 900,000) and ethanol 99% were purchased from Sigma-Aldrich. Solvents, including dichloromethane (DCM) and dimethyl formamide (DMF), were purchased from Union Chemical Works, Ltd., and Macron Fine Chemicals. Silver nitrate was acquired from Wako Pure Chemical Industries, Ltd. for the synthesis of silver nanoparticles. HRSE flowers of the red varietal were picked from the campus garden at National Taiwan University, Taiwan (Fig. 1). The standards used for compound identification in HRSE flowers include cyanidin-3-o-glucoside (Nature Standard, China), cyanidin-3-sambubioside, cyanidin-3-sophoroside, delphinidin-3-glucoside, and delphinidin-3-sambubioside (Phytolab, Vestenbergsgreuth, Germany). Other standard compounds listed in Table S1 were also purchased from Phytolab. The food model used in this study, which was *Exopalaemon orientis* (Holthuis, 1950), is a shrimp of commercial importance in Taiwan. They were caught from freshwater in Pingtung Province of Taiwan and were immediately packed in ice and stored at −60 °C within 3 h (FishAniki®, Tainan, Taiwan).

2.2. Preparation of the anthocyanin extract (AE), compound identification, and quantification

Flowers of HRSE were frozen overnight and freeze-dried for 72 h. The lyophilized flower petals were crushed and dipped in 99% ethanol in a 1:20 (w/v) ratio. The mixture was stirred vigorously for 24 h at room temperature (23 ± 2 °C), and the supernatant containing anthocyanin was collected after centrifugation. This supernatant will be called anthocyanin extract (AE) throughout this study.

UPLC-MS/MS was performed to identify the significant anthocyanin compounds in the AE of HRSE. The analysis was performed on a calibration range of 10–100 ng/mL. The system was built on the Waters Acquity UPLC platform and Waters Triple Quadrupole Mass Spectrometry (TQS) operated in positive electrospray ion (ESI) mode. A Phenomenex Kinetex Biphenyl (100 Å, 1.7 μm, 2.1 mm × 100 mm) column was incubated at 35 °C with a flow rate of 0.3 mL/min and a sample injection volume of 2 μL. The AE was diluted with methanol 100-fold before injection. The mobile phase was composed of ddH_2O and acetonitrile, both containing 0.1% (v/v) formic acid. The linear gradient conditions of the mobile phase start with 20% acetonitrile and end with 30% acetonitrile within 10 min. The running parameters for ESI include 3.2 kV capillary voltage, 19 V cone voltage, 300 °C desolvation temperature, 150 °C source temperature, 700 L/h desolvation gas flow, 150 L/h cone gas flow, 7.0 bar nebulizer gas flow, and 50 to 700 Da scan range (m/z). The MS/MS data for the anthocyanins were collected by multiple reaction monitoring (MRM) mode in MassLynx4.1 software. The optimized MRM conditions for standard compounds are shown in Table S1.

2.3. Sensor membrane fabrication

A stepwise procedure for fabricating the colorimetric pH sensor is shown in Fig. 1. Both of the polymers for sensor fabrication, PCL (3% w/v) and PEO (3.5% w/v), were prepared in a mixture of solvents containing DMF and DCM in a 4:1 ratio. The as-prepared PCL and PEO were then mixed at ratios of 1:1, 1.5:0.5, 1.6:0.4, and 1.8:0.2 (v/v), followed

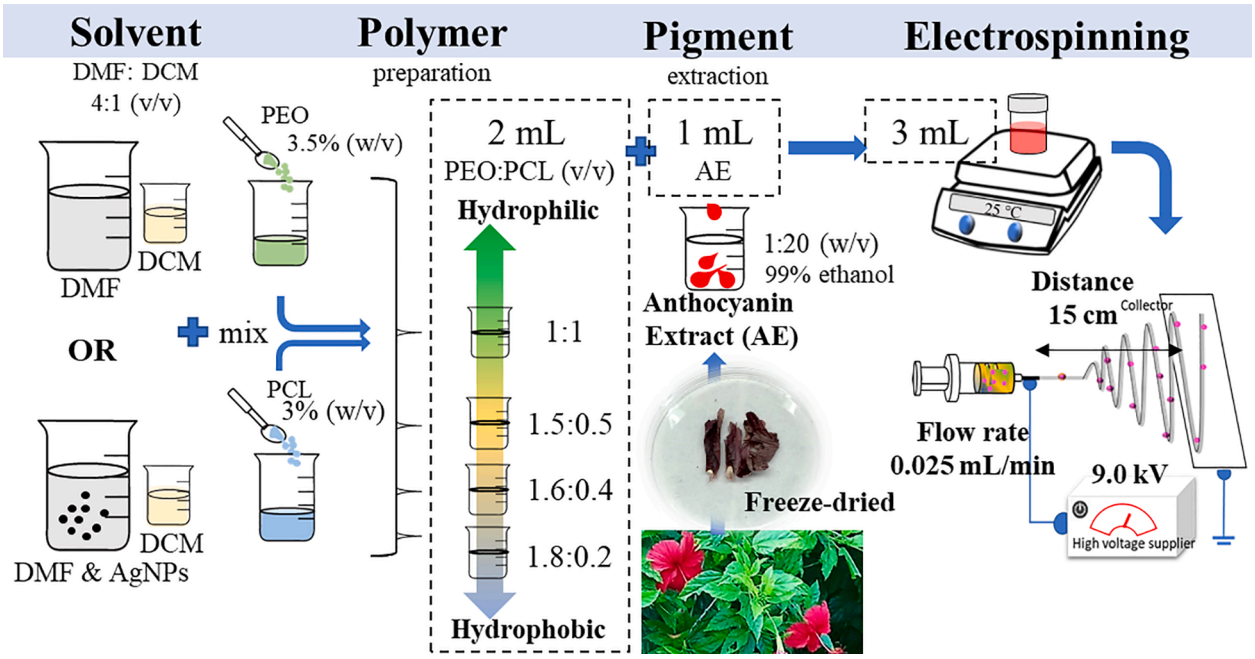

Fig. 1. A stepwise procedure for fabricating the colorimetric pH sensor. Major steps include solvent and polymer preparation and the incorporation of AE into the electrospun fibers.

by the addition of 1 mL of AE (318 mg/mL cyanidin-3-o-glucoside and 2 mg/mL cyanidin-3-sophoroside in ethanol, as shown in Table 1). One mL of ethanol was added to the 2-mL polymer mixtures as a control to make PCL-PEO fibers. These procedures brought the volume of all the material mixtures to a total of 3 mL.

In the fabrication of fibers containing silver nanoparticles (AgNPs), the procedure starts with the mixing of 0.2% (w/v) silver nitrate in DMF, one of the solutions for polymer preparation mentioned above. This previously characterized reducing agent, DMF, reduces silver ions into AgNPs (Pastoriza-Santos & Liz-Marzán, 2000). The formation of AgNPs in DMF could be confirmed by measuring the absorbance peak intensity at approximately 430 nm on the UV–visible spectrum (data not shown). The AgNP-containing DMF was then mixed with DCM in a 4:1 ratio, which served as a solvent for preparing the PCL (3% w/v) and PEO (3.5% w/v) polymer solutions. This time, the as-prepared PEO and PCL solutions containing AgNPs were mixed in an exact 1.6:0.4 (v/v) ratio with 1 mL of AE.

Table 1
Cyanidin-3-sophoroside and cyanidin-3-glucoside contents in different plants.

Sample	Solvent for extraction	Cyanidin-3-sophoroside (mg/mL)	Cyanidin-3-glucoside (mg/mL)	Ratio
Sour cherry (*Prunus cerasus*)[1]	Ethyl acetate	11.07 ± 0.8	10.06 ± 0.3	1.1: 1
Red raspberry (*Rubus idaeus*)[1]	Ethyl acetate	239.4 ± 2.8	42.5 ± 0.7	5.6: 1
Montmorency cherry (*Prunus cerasus* L. cv. Montmorency)[2]	Ethanol	1.88	0.29	6.5: 1
English Morello cherry (*Prunus cerasus* L.)[2]	Ethanol	7.78	2.69	2.9: 1
Hibiscus flower (*Hibiscus rosa-sinensis*) [3]	Ethanol	318.1	2.10	151.5: 1
	Methanol	396.3	1.36	291.4: 1

[1] (Jakobek et al., 2009).
[2] (Chandra, Nair, & Iezzoni, 1993).
[3] This study.

The freshly prepared gel polymer solution was fed into a 5-mL Terumo plastic syringe fitted with a 23G microtip needle connected to a high-voltage power supply (Falco, Model FES-HV30, Taiwan) with the applied voltage set at 9.0 kV. The gel polymer solution was delivered to the spinneret with an infusion pump (New Era Pump Systems, Model NE-300, U.S.A.) at a 0.025 mL/min flow rate. The distance between the needle tip and the plate collector spinneret was set at 15 cm. The thickness of the fiber mat was controlled through the spinning time. Each fiber mat was collected from the plate collector after 2 h of electrospinning.

The color difference between two colors was expressed as the total color difference (ΔE) with Eq. (1).

$$\Delta E = \left(\Delta L^2 + \Delta a^2 + \Delta b^2\right)^{1/2} \quad (1)$$

where ΔL, Δa, and Δb represent the differences in brightness, redness, and yellowness, respectively, between two colors.

2.4. Fiber characterization

The fiber morphology and fiber diameter of the randomly selected parts of the nanofiber scaffolds were analyzed by a thermal field emission scanning electron microscope (SEM, JEOL JSM-7800F) and ImageJ software (National Institute of Health, NIH, Maryland, USA), respectively. Fourier transform infrared spectroscopy (FTIR, Bruker Optik, Ettlingen, Germany) was performed in the range of 650–4000 cm^{-1} to define the existence of the components among fibers and materials. In addition, the presence of AgNPs in nanofibers was confirmed by transmission electron microscopy (TEM, Hitachi H-7100) and X-ray diffraction (XRD, Bruker D2 PHASER) method. The fibers for TEM analysis were collected on a copper mesh that was attached to the collector plate during electrospinning. The wettability of the fiber scaffolds was determined by measuring the water contact angle between a water drop and the fiber. Specifically, a ten-microliter drop of deionized water was placed on the fiber surface, and the process was recorded on a camera (Alpha A7S II, Sony). The angle at which the droplet remained for a few seconds on the mat before being completely absorbed was determined to be the contact angle. The contact angle formed between the droplet and the mat was calculated using ImageJ to determine the hydrophobicity or

hydrophilicity of the membrane (Kuntzler et al., 2020).

2.5. Packaging test and determination of quality parameters

These pH-sensing electrospun fibers were used in shrimp packaging to monitor quality changes during storage. For this, ten shrimp were evenly arranged in a Petri dish (60 mm × 15 mm) without an absorption pad and were sealed directly using a polyethylene film with a circular shape indicator (1 cm in diameter) attached to the side of the film using a transparent double-sided tape (0.3 cm in diameter). The packaged shrimp were stored at different temperatures (25 °C, 10 °C, and 4 °C) with light exposure (980 ± 78 lx of average luminous intensity, Sylvania T8 Luxline Plus F36W/840, 4000 K – Cool White color temperature). The CIELab values of the indicator (*L*-value: lightness, *a*-value: redness and greenness, *b*-value: yellowness and blueness) were measured from the images obtained from a chromameter. For pH measurements as well as other quality parameters during storage, ten shrimps stored under the same conditions mentioned above were homogenized in a stomacher bag containing 20 mL of distilled water, and the pH was measured using a pH meter. Other parameters, such as TMA-N analyses, were conducted by extracting TMA-N in a single trichloroacetic acid (TCA) extraction from the homogenized product of shrimp, and the level was determined by a spectrophotometer (V-650 UV–VIS Spectrophotometer, JASCO) at a wavelength of 410 nm (Erkan, 2007). The level of indole was determined by the modified colorimetric method (Cheuk & Finne, 1981). The microbiological features of the shrimp during monitoring were recorded through the testing of TMC in shrimp using 3 M™ Petrifilm™ (3 M Microbiology, St. Paul, MN), which was used according to the manufacturer's instructions.

2.6. Data analysis and calculation of activation energy

The color of the pH sensor is related to the shrimp quality degradation parameters during storage. These correlations could be confirmed by matching the similarities among the activation energies (Ea) of the quality parameters. Good sensors should faithfully present the status of food quality. Therefore, it is widely accepted that the difference in Ea values between sensors and food quality parameters should be no more than 25 kJ/mol (Choi, Jung, Lee, & Lee, 2014). To calculate Ea values, the levels of the color change of the pH sensor and the change of quality parameters related to food deterioration during shrimp storage at different temperature must be first plotted into figures as a function of time (*t*). This allows us to obtain the reaction rate constant (k) of each food quality parameter according to the best curve fitting result. The parameter of the k value obtained at different temperatures can then be used to plot lines according to the Arrhenius equation (Eq. (5)), and Ea is calculated. The equations shown below are used to determine the k value at different temperatures (Kim, Choi, Kim, Kim, & Lee, 2013).

$$Zero-order\ reaction: Y = k_T\ t + Y_0 \tag{2}$$

$$First-order\ reaction: Y = e^{k_T \times t} \tag{3}$$

Y and Y_0 are the response variables of TMA-N, indole, TMC, or pH and their initial levels, respectively. k_T represents the reaction rate constant ($hours^{-1}$) at a certain temperature (T). *t* is the reaction time (hours).

$$Gompertz\ equation: b(t) = \Delta b \times exp\ (-exp\ (-(t - t_0 \times k_T)) + b_0 \tag{4}$$

b (*t*) is the value of the *b* CIELab parameter for time *t* (hours), Δb is the *b*-value amplitude during monitoring lifetime, b_0 is the *b* value at zero hours, and k_T is the reaction rate at temperature T (Zabala, Castán, & Martínez, 2015).

$$Arrhenius\ equation: \ln k = Ea/(RT) + \ln A \tag{5}$$

Ea is the activation energy (kJ/mol), R is the universal gas constant (0.008314 kJ/mol K), T is the absolute temperature, and A indicates the pre-exponential factor (h^{-1}).

3. Results and discussion

3.1. Anthocyanin identification

The possible anthocyanins in the HRSE extracted by methanol or ethanol were analyzed and compared. UPLC-MS/MS analyses revealed that the anthocyanins found in both extracts matched two out of the five common anthocyanin standards (Table S1 and Fig. S1a), cyanidin-3-o-glucoside and cyanidin-3-sophoroside. This result echoed a previous study showing that cyanidin-3-sophoroside is the main anthocyanin of HRSE (Vankar & Shukla, 2011). The work also confirmed that the sample was indeed the stated species used in this study and not confused with Roselle (*Hibiscus sabdariffa*), a species commonly associated with *Hibiscus* tea production. The major anthocyanins found in *H. sabdariffa* are cyanidin-3-sambubioside and delphinidin-3-sambubioside (Pinela et al., 2019). Aside from the *Hibiscus* flower, some cherry strains (*Prunus cerasus*) and red raspberry (*Rubus idaeus*) also contain both cyanidin-3-sophoroside and cyanidin-3-glucoside (Chandra, Nair, & Iezzoni, 1993; Jakobek, Šeruga, Šeruga, Novak, & Medvidović-Kosanović, 2009). Neither component is the primary anthocyanin compound in cherry strains, while cyanidin-3-sophoroside is the main anthocyanin component for red raspberry. Even so, the ratio of cyanidin-3-sophoroside to cyanidin-3-glucoside was unique in HRSE (Table 1). The anthocyanins extracted by ethanol were chosen for further applications other than methanol extract for food safety issues.

Here, we report the existence of other compounds in the HRSE AE. The results shown in the chromatograms of ultra-performance liquid chromatography-quadrupole time-of-flight (UPLC-QToF) in positive and negative ionization modes were quite similar to the above UPLC-MS/MS results, in which cyanidin-3-sophoroside and cyanidin-3-glucoside were the major anthocyanins in the diluted AE samples (Fig. S1b). However, several compounds including rutin, hyperoside, isoquercetin (isoquercitrin), quercetin, kaempferol, and gallic acid, were detected in AE samples without dilution (Table S1 and Fig. S1b lower panel). Previously, rutin was involved in copigmentation (Fan, Wang, Xie, Zhang, Li, & Zhou, 2019); Phenolic acids, such as gallic acid, showed evident copigmentation and sometimes stabilized anthocyanins (Su, Xue, Yang, Deng, Meng, & Guo, 2017); Isoquercetin was able to protect anthocyanins from UV light damage (Wu, Cui, Huang, Fu, & Jin, 2016). Therefore, the existence of these minor compounds may result in possible copigmentation of HRSE AE.

3.2. Fiber characteristics

Different proportions of PCL and PEO polymer solutions with the same amount of AE were made to obtain the best color responses to pH buffers. PCL introduces hydrophobicity, while PEO is responsible for the hydrophilicity of the fiber. The ratios of the two polymers were adjusted to produce a membrane that can absorb liquid samples while maintaining water resistance. The increment of PCL prevents the pigments from leakage, while a ratio that is too high repels water absorption with a less noticeable color response to pH buffers (Table S2).

Researchers previously showed that the color difference was evident for ΔE values between 3.5 and 5. By values of ΔE greater than 5, the observer detects two colors (Mokrzycki & Tatol, 2011). Therefore, the color response significances of the indicator made from different formulas could be quantitatively compared through the calculation of ΔE (Eq. (1)). The ΔE in Fig. 2a was to show the color response significance before and after buffer treatments. The most significant color response could be seen on the membrane fabricated at a PCL and PEO ratio of 1.6:0.4, which had the highest ΔEs throughout every tested pH treatment except for the color at pH 7 (values of ΔE are shown in the first row of Table S3 with the "e1" superscript). In addition, to guarantee perceptible color changes from one pH to the adjacent pH. The ΔEs

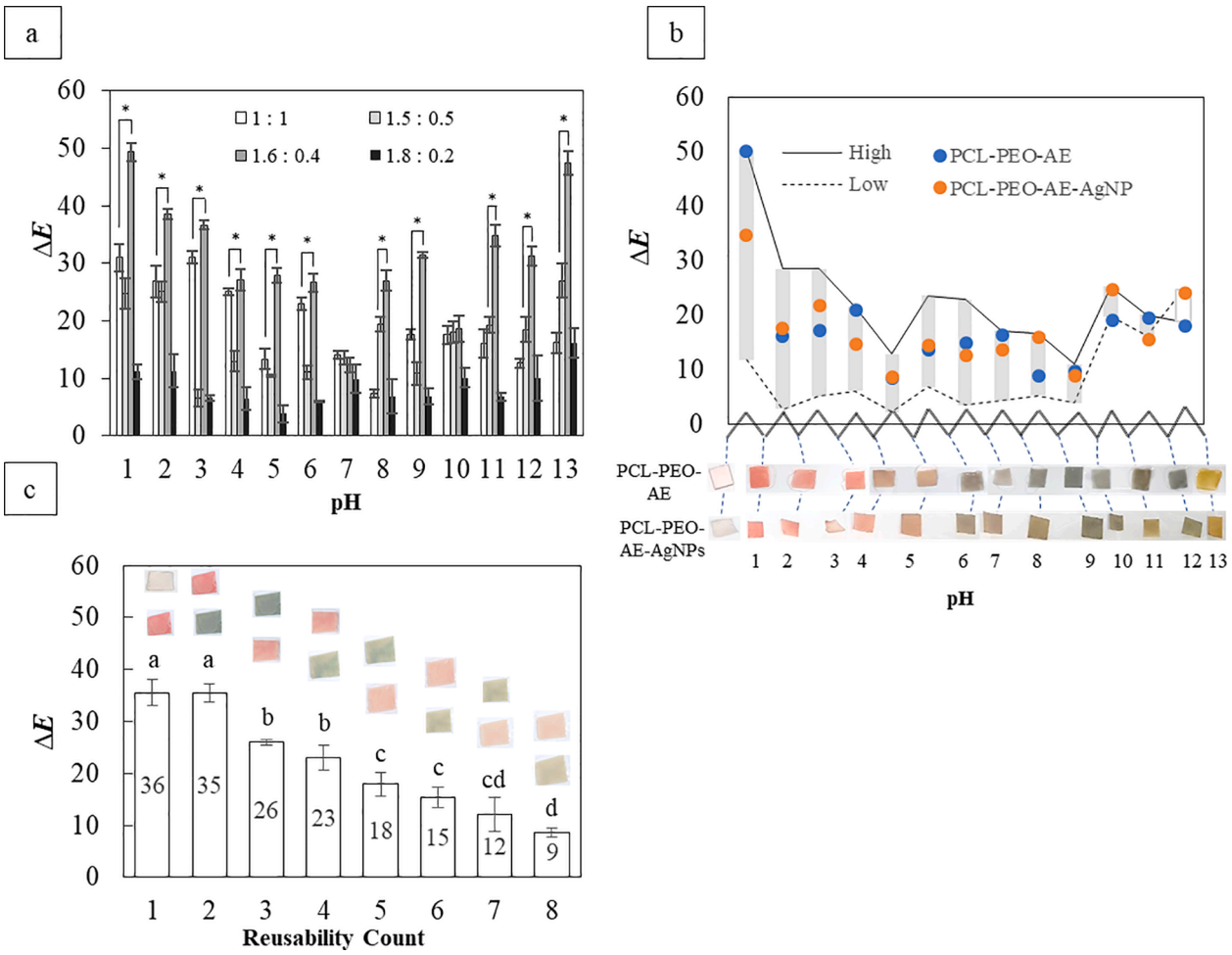

Fig. 2. The total color difference (Δ*E*) as a function of pH for the electrospun fibers made from different ratios of PCL:PEO polymers embedded with AE. The Δ*Es* from this plot were calculated from the color differences of the indicator with and without buffer treatment at each pH. * Significantly higher Δ*E* compared to the second-highest Δ*E* ($p < 0.05$ for Student's *t*-test) (a); Δ*E* values observed for each pH with respect to other pH values linked with two doubled lines in membranes (PCL: PEO in a 1.6:0.4 ratio) w/wo AgNPs. The high and low boundaries of the relative Δ*E* values compared among studies (b); the Δ*E* values of the pH sensing membrane at extreme pH conditions showing the color reversibility against pH 1 and 10; means with different lowercase letters are significantly different ($p < 0.05$ for analysis of variance (ANOVA), followed by Tukey's test) (c).

between each indicated color of the sensor at different pH buffer treatment (dashed line) were calculated. These Δ*Es* all either located within or at the high and low boundaries of the Δ*Es* mentioned in this and other studies, which were all greater than 5 (Fig. 2b, and the numbers of Δ*Es* are shown in the gray-shaded areas of Table S3 with an "e1 or e2" superscript), indicating that the colors developed at different pH values belong to different color spaces and can be easily distinguishable from one another by the naked eye.

The membrane reusability test can be performed under extreme pH conditions (Devarayan & Kim, 2015). The color of the pH sensor was recorded once the membranes were treated with buffer at pH 1. This procedure was followed by drying the membrane with tissue paper and treatment with alkaline buffer at pH 12. The tests were repeated until membranes no longer showed any significant color changes. The Δ*E* remained greater than 5 after eight rounds of repetitive tests (Fig. 2c), suggesting the robustness of the pH sensor.

The SEM images revealed that the morphology of PCL-PEO fibers tended to be porous, which can be reduced with the addition of AE (Fig. 3a). The addition of AE also reduced the average diameter of fibers from 1220 nm for PCL-PEO to 457 nm for PCL-PEO-AE. The addition of AgNPs to PCL-PEO polymers also reduced the fiber diameter. The average diameter of PCL-PEO fibers was reduced from 1220 nm to 751 nm in PCL-PEO-AgNP fibers. A previous study showed that the addition of AgNPs increased the conductivity of the solution (Lee, Jeong, Baek, & Youk, 2005), which resulted in jet elongation and solidification, causing the fiber to dry quickly without adhesion. High conductivity also leads to finer fiber formation (Zhang, Yuan, Wu, Han, & Sheng, 2005). Even so, the fibers without AE were larger in diameter than their counterparts, which contained AE. The average diameter of the PCL-EO-AE-AgNP nanofibers was 472 nm (Fig. 3a).

PCL is a hydrophobic polymer and is commonly used to fabricate water-resistant membranes. It is necessary to use PCL as the base for the pH indicator, as it prevents the sensors from breaking down upon contact with the liquid sample. However, the product should absorb water to allow the samples to contact AE embedded in the fiber. Therefore, PEO was added to increase the hydrophilicity of the membrane. As seen in the inset of Fig. 3a, the water contact angle for all samples was less than 90°, indicating that all mats tend to be hydrophilic and allow the spread of the water. Complete wetting occurs on mats with a water contact angle of 0°. Moreover, a contact angle larger than 90° indicates that the mat is hydrophobic; therefore, water will form droplets on its surface (Yuan & Lee, 2013). A hydrophilic membrane allows liquid sample to spread across its surface, a characteristic that is favored for a pH indicator.

In the FTIR spectra, PEO and PCL have sharp peaks at 3500 cm^{-1} (N—H stretching), 2926 cm^{-1} (C—H stretching), 1728 cm^{-1} (C═O

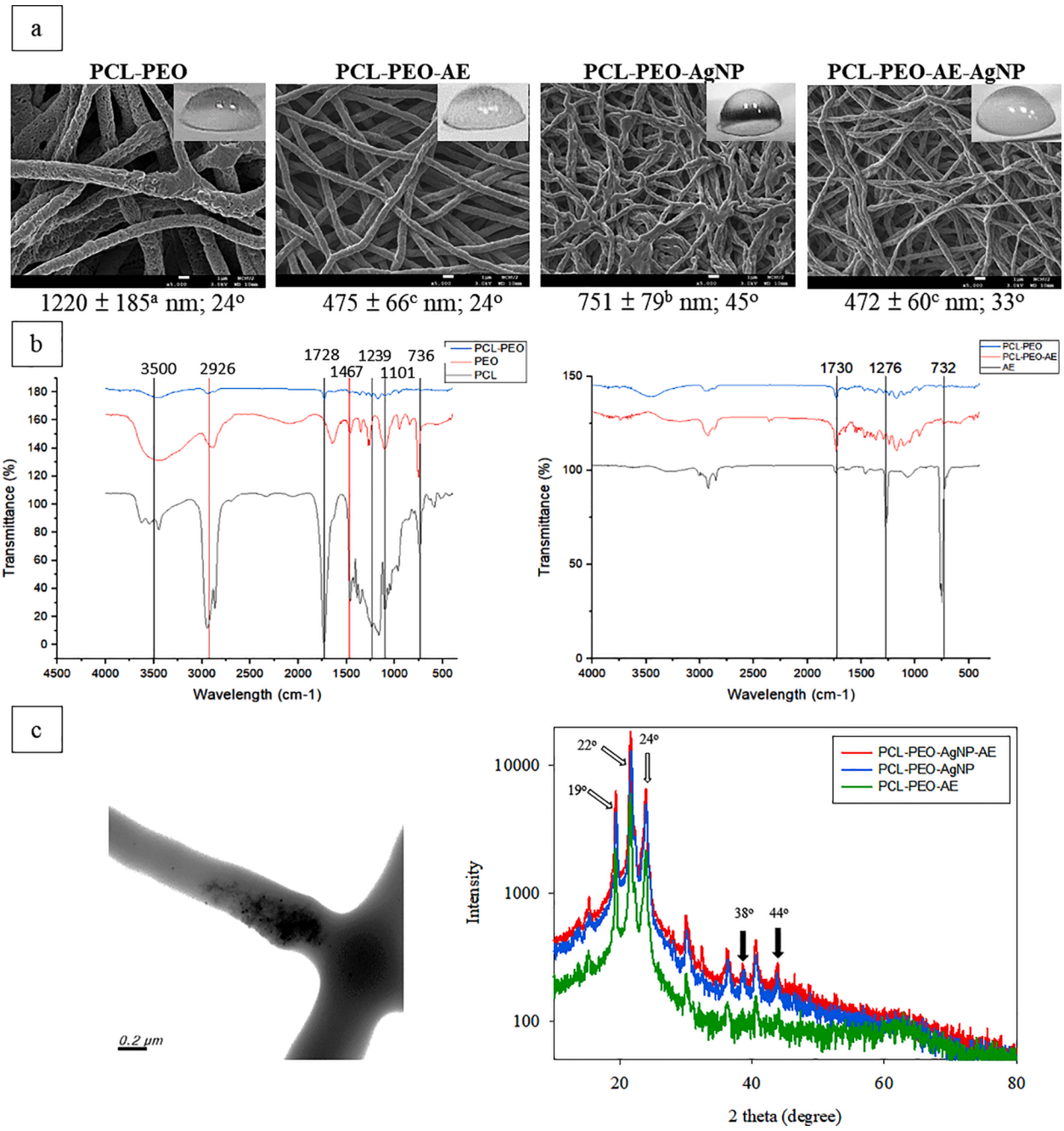

Fig. 3. Fiber characterization. SEM images, fiber diameter (nm), and contact angle of the electrospun fibers. Means with different lowercase letters are significantly different ($p < 0.05$ for analysis of variance (ANOVA), followed by Tukey's test) (a); FTIR spectra of the electrospun fiber mats (b); TEM images of fibers containing AgNPs and the XRD results for fiber analyses. White arrows point at peaks of 22° and 24°, representing the crystal structure of PCL, and 19° and 24° for crystal structure of PEO. Peaks at 30° to 80° degrees highlighted by black arrows indicate signals of AgNPs.

stretching), 1467 and 736 cm^{-1} (–CH_2 stretching) as well as 1239 and 1101 cm^{-1} (C—O stretching) (De Paula et al., 2018). All the characteristic peaks of PEO and PCL decreased after mixing the two polymers (Fig. 3b, left panel). A sharp peak at 1276 cm^{-1} in the AE sample (Fig. 3b, right panel) represents the stretching vibrations of the phenol pyran ring in AE (Moradi et al., 2019). A similar pattern of peak absorbance was observed with the addition of AgNPs to polymers for fiber formation (Fig. S2).

As seen in the left panel of Fig. 3c, AgNPs were randomly distributed inside the electrospun fibers, in which the particles were either arranged within clusters or individually separated. ImageJ analysis revealed that the diameter of AgNPs was 20–30 nm. The right panel of Fig. 3c shows the XRD results for fiber analyses and reveals that all fibers containing PCL have signals peaking at approximately 22° and 24°. These peaks reflected the (110) and (200) planes of PCL's orthorhombic crystal structure (Borjigin et al., 2013). PEO peaks could be found at 19° and 24° in the XRD chart, and the latter overlapped with the PCL. The peaks exhibited the semicrystalline structure of PEO (Bhide & Hariharan, 2007). Peaks at 30° to 80° indicate the presence of AgNPs. Specifically, the two peaks pointed out by the black arrows at 38° and 44° were the (111) and (200) planes of crystalline silver, respectively (Shameli et al., 2012).

The presence of AgNPs in fibers could also be confirmed by their synergistic effect with AE on inhibiting the growth of bacteria (Fig. S3).

Qin (2019) also noticed the synergistic killing effect on bacteria between AgNPs and anthocyanins extracted from purple corn (Qin, Liu, Yuan, Yong, & Liu, 2019). To the best of our knowledge, few pH indicators have been made with antimicrobial activity. The purpose of fabricating antimicrobial fibers was to retard the growth of microbes directly on the sensor, which would affect the sensing accuracy.

3.3. Kinetics of the color change response and shrimp quality changes

New compounds and metabolites from microbial growth accumulate as food deteriorates. This is true for seafood, as it deteriorates with changing pH value, along with the formation of various compounds. However, before applying our colorimetric pH sensor to indicate the freshness of the food product, the correlations between pH level and other quality parameters during food storage needed to be investigated. In other words, matching the color change of the colorimetric pH sensor with other food quality parameters would enable us to determine whether the color of the indicator can be used to reflect the quality of the food product. The quality of seafood products could be determined through the inspection of the levels of TMA-N, indole, pH, and TMC according to the pre-established standards from sensory perception and hygienic regulations. Therefore, we can match the quality parameters mentioned above with color changes of the indicator by calculating their respective reaction rate constant (k) first during food storage followed by Ea calculation, the processes for which are mentioned in the following section.

The shrimp quality during storage was monitored using the packaging settings with the colorimetric pH sensors shown in Fig. 4a. The sensors changed colors as the shrimp deteriorated (Fig. S4). The color-changing response of the sensor could be detected visually in the first 100 h of shrimp storage at 4 °C, in which the Δ*E* values calculated between each adjacent color square as a reference were also proven to be greater than 5 (Fig. 4b). However, it is difficult to use the Δ*E* values for matching of quality parameters. In other words, it is impossible to obtain the k value of Δ*E* because it appears to be a better parameter to show the level of color differences between two colors. For example, if a foodstuff changes its pH from 1 to 13 during storage, the color of the pH sensor would change from red to brown, which resembles a "U-shaped" curve in Fig. 2a. The U-shaped curve of Δ*E* values neither positively nor negatively correlates with the time course, which makes it difficult to obtain a fixed k value, the rate constant. Moreover, according to our results of the color of the sensor response during shrimp storage, there were minimal changes in the *L and a* parameter of the CIELab system used to calculate the Δ*E* (Fig. S4b), and we were unable to calculate the respective k values of the two parameters. Therefore, the representative color change measured in the *b* parameter of the CIELab system was used to calculate the color change k value throughout storage, in which the change follows the Gompertz model, as shown in Table 2. The metabolites produced over the time course of shrimp storage, including TMA-N and indole, as well as the changes of pH were determined, which all followed the zero-order reaction (Kim et al., 2013); However, the first-order reaction was found to be the best fit of the bacterial growth kinetics (Kim et al., 2013). These best fitting results allowed us to obtain the k values of each parameter.

After confirming the temperature-dependent k values of each parameter, as shown in the equations in Table 2 with an underline mark, the Ea values can be calculated using the Arrhenius equation (Eq. (5)). The Ea values of TMA-N, indole, TMC, and pH were estimated to be 24.62 kJ/mol, 27.14 kJ/mol, 30.75 kJ/mol, and 20.59 kJ/mol, respectively. The matching similarities among the Ea values of quality

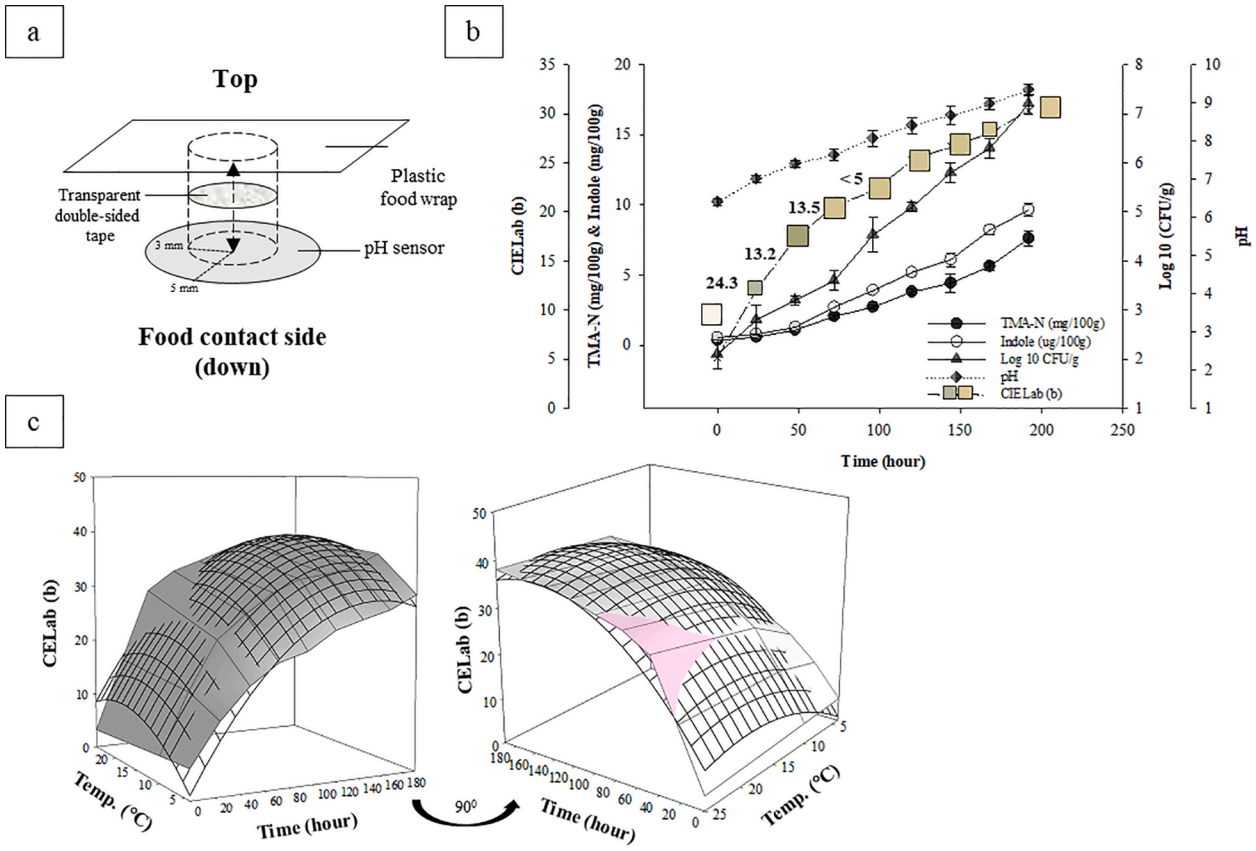

Fig. 4. The package settings for food monitoring and the fabrication layouts of the colorimetric pH sensors (a). Changes in quality parameters in shrimp during isothermal storage conditions at 4 °C; data points in the *b* parameter curve are substituted with color squares observed on the sensor, and the numbers between two color squares indicate the total color difference values (Δ*E*) between squares and squares at the previous time point (b). Response surface plot of CIELab (*b* parameter) versus temperature and time for the colorimetric pH sensors (c).

Table 2
Reaction rate constants (k) and activation energies (Ea) of shrimp of different quality parameters during storage at different temperatures.

List	Reaction order	Temperature (°C)	Equation	R^2	Ea (kJ/mol)	R^2
TMA-N (mg/100 g)	Zero	4	0.0365 t − 0.3715	0.96	24.62	0.96
	(Eq. (2))	10	0.0398 t − 0.2604	0.97		
		25	0.0751 t + 0.2627	0.96		
Indole (μg/100 g)	Zero	4	0.0491 t − 0.4526	0.97	27.14	0.97
	(Eq. (2))	10	0.0732 t − 0.5715	0.98		
		25	0.1166 t − 0.0183	0.97		
TMC (Log_{10} CFU/g)	First	4	2.3066 e exp 0.0062 t	0.98	30.75	0.98
	(Eq. (3))	10	2.6147 e exp 0.0073 t	0.95		
		25	2.1713 e exp 0.0154 t	0.97		
pH	Zero	4	0.0144 t + 6.6	0.99	20.59	0.99
	(Eq. (2))	10	0.0173 t + 6.583	0.98		
		25	0.027 t + 6.8587	0.94		
CIELab parameter (b)	Gompertz equation	4	27.1111 × exp(-exp(-(t-8.1165) × 0.0538))-0.6131	0.97	20.23	0.99
	(Eq. (4))	10	29.5678 × exp(-exp(-(t-23.6868) × 0.0612)) + 4.1471	0.98		
		25	32.2017 × exp(-exp(-(t-28.2984) × 0.09859)) + 3.1615	0.98		

The reaction rate constants (k) are underlined in each equation.

parameters reveal the correlations among them during shrimp storage. The results showed that the Ea of the color response of the *b* parameter was 20.23 kJ/mol, which was more closely related to the Ea value of the measured pH than other shrimp quality parameters. A previous study showed that the difference in Ea between food sensors and food deterioration parameters should be less than 25 kJ/mol, which indicates that the sensor correctly indicates the quality of the food being monitored (Choi et al., 2014). Additional research suggests that the Ea difference should be less than 10 kJ/mol for the sensor to determine the correct shelf life (Mataragas, Bikouli, Korre, Sterioti, & Skandamis, 2019). The Ea differences among the colorimetric pH sensor and other food deterioration parameters (except the TMC) obtained in this study were all less than 10 kJ/mol, suggesting that the colorimetric pH sensor could not only determine the pH but also simultaneously reflect several quality parameters of shrimp. In addition, the Ea of the colorimetric pH sensor created in this study was comparable to the Ea value of the color reaction sensors developed by Jhuang, which was 24.2 ± 0.6 kJ/moL (Jhuang et al., 2020), indicating that the color change reaction easily initiates without chemical hindrance or time delay. In addition to the match of Ea, the Pearson correlation coefficient (R) analysis results also indicate high correlations between the *b* parameter and other quality parameters (Table S4). Therefore, the colorimetric pH sensor reflects the quality of the shrimp that is being monitored.

To view this colorimetric pH sensor from another perspective, the possibility of its usage in predicting the shelf life endpoint of food products could be realized through mathematical modeling (Gao, Tian, Zhu, & Sun, 2020). A three-dimensional response surface plot was constructed to simulate the time–temperature response of the *b* parameter in the CIELab system (Fig. 4c). The following regression equation was obtained from the reaction diagram:

$$Y = 0.3666\ X_1 + 1.6771\ X_2 - \ 0.0012\ X_1^2 - \ 0.0453\ X_2^2 - 5.12,\ R^2 = 0.9282\ (p < \ 0.05.) \quad (6)$$

Y, X_1, and X_2 represent the *b* parameter of the CIELab system, time (hours), and temperature (°C), respectively.

The above regression equation reliably indicates the situation of shrimp during storage at different temperatures. This means that the amount of time for shrimp quality to reach an unacceptable level can be known at a specific temperature. For example, in accordance to Eq. (6), the *b* parameter at 30.32 was reached after 192 h of shrimp storage at 4 °C. However, the same endpoint of *b* was reached less than 96 h when the reaction temperature was 25 °C. Thus, the higher the temperature, the more likely the color change reaction reached certain point, which correlates to the deterioration process of shrimp. However, a more acceptable endpoint of *b* should be suggested to accurately predict the shelf life of the shrimp store at different temperatures.

The guidelines established for the acceptability of shrimp at different storage temperatures suggest that the quality parameters, including pH, TMA-N, and indole, should be no more than 7.5, 5.0 mg/100 g, and 9.0 μg/100 g, respectively (Shamshad, Riaz, Zuberi, & Qadri, 1990). According to this, 20 would be suggested as the threshold of the *b* parameter in the CIELab system to put into Eq. (6). and to estimate the maximum shelf life of shrimp stored at different temperatures. For the shrimp stored at 4, 10, and 25 °C, the maximum shelf life was 72, 48, and 37 h, respectively. However, shrimp are not acceptable after storage for 37 h at room temperature. As we take a closer look at the left panel of Fig. 4c, turning the original plot at 90° to the right, there is a significant hump above the modeled curve surface (curve surface formed by grids) at 25 °C when the *b* parameter is at the threshold of 20, indicating an underestimation of the real *b* parameter that results in a more extended prediction of shelf life at room temperature. Therefore, we suggest that the predictive model for shelf life endpoint determination shown in this study only works at a lower temperature. A reference color table derived from real samples can be used to show the freshness/spoilage status of shrimp stores at 4 °C and 10 °C (Table S5). It is feasible to distinguish fresh and spoiled shrimp as the ΔE were all greater than 5. However, a more careful inspection must be made to differentiate between colors of indicators indicating different levels of freshness or between medium fresh and spoiled shrimp as the ΔE gradually decreased (from 24.3 to 1.8 in Fig. 4b).

4. Conclusion

This study successfully demonstrated that PCL and PEO polymers are desirable carriers for anthocyanin extracts and silver nanoparticles in the process of synthesizing electrospun fibers. The double network polymers adjusted the hydrophobicity and hydrophilicity of fibers that interacted with liquid samples appropriately and retained most pigments without leakage during most pH monitoring situations. The colorimetric pH sensor made from these fibers responded to different pH values with a unique color code and ΔE values in a detectable range by the human eye. When used in food monitoring, the sensor could be attached to the food warping cover as an on-pack biosensor and would change color during shrimp storage. The *b* parameter obtained in the color change could further project the shrimp's quality and could be used to predict the shelf life of shrimp through our established three-dimensional kinetic model, especially under refrigeration temperatures. However, a specific reference color guide is required to inform consumers about the deterioration of a specific food since every food has its own unique deterioration scenario. Even so, the proposed indicator can remain sensitive to pH fluctuations and may be incorporated into smart food packaging.

CRediT authorship contribution statement

Lavernchy Jovanska: Data curation, Writing - original draft, Visualization, Formal analysis. **Chun-Hui Chiu:** Visualization, Investigation. **Yi-Cheun Yeh:** Writing - review & editing, Resources, Funding acquisition. **Wen-Dee Chiang:** Resources. **Chang-Chi Hsieh:** Resources, Validation. **Reuben Wang:** Conceptualization, Methodology, Writing - review & editing, Supervision, Project administration, Funding acquisition.

Declaration of Competing Interest

The authors declare that they have no known competing financial interests or personal relationships that could have appeared to influence the work reported in this paper.

Acknowledgments

The Ministry of Science and Technology of Taiwan supported this work (MOST 109-2221-E-002-206-MY3 and MOST 107-2113-M-022-025-MY4). Thanks to Professor Chao-Sung Lin, Ms. Yuan-Tzu Lee, and Mr. Hsueh-Ren Chen of Instruentation Center,National Taiwan University for the assistance in SEM and TEM experiments.

Appendix A. Supplementary data

Supplementary data to this article can be found online at https://doi.org/10.1016/j.foodchem.2021.130813.

References

Bhide, A., & Hariharan, K. (2007). Ionic transport studies on $(PEO)_6$: $NaPO_3$ polymer electrolyte plasticized with PEG_{400}. *European Polymer Journal, 43*(10), 4253–4270. https://doi.org/10.1016/j.eurpolymj.2007.07.038.

Borjigin, M., Eskridge, C., Niamat, R., Strouse, B., Bialk, P., & Kmiec, E. B. (2013). Electrospun fiber membranes enable proliferation of genetically modified cells. *International Journal of Nanomedicine, 8*, 855. https://doi.org/10.2147/IJN.S40117.

Burton-Freeman, B. M., Sandhu, A. K., & Edirisinghe, I. (2016). Red raspberries and their bioactive polyphenols: cardiometabolic and neuronal health links. *Advances in Nutrition, 7*(1), 44–65. https://doi.org/10.3945/an.115.009639.

Chandra, A., Nair, M. G., & Iezzoni, A. F. (1993). Isolation and stabilization of anthocyanins from tart cherries (*Prunus cerasus L.*). *Journal of Agriculture and Food Chemistry, 41*(7), 1062–1065. https://doi.org/10.1021/jf00031a009.

Cheuk, W. L., & Finne, G. (1981). Modified colorimetric method for determining indole in shrimp. *Journal of the Association of Official Analytical Chemists, 64*(4), 783–785. https://doi.org/10.1093/jaoac/64.4.783.

Choi, D. Y., Jung, S. W., Lee, D. S., & Lee, S. J. (2014). Fabrication and characteristics of microbial time temperature indicators from bio-paste using screen printing method. *Packaging Technology and Science, 27*(4), 303–312. https://doi.org/10.1002/pts.2039.

De Paula, M. M. M., Bassous, N. J., Afewerki, S., Harb, S. V., Ghannadian, P., Marciano, F. R., et al. (2018). Understanding the impact of crosslinked PCL/PEG/GelMA electrospun nanofibers on bactericidal activity. *PLoS ONE, 13*(12), e0209386. https://doi.org/10.1371/journal.pone.0209386.

Devarayan, K., & Kim, B.-S. (2015). Reversible and universal pH sensing cellulose nanofibers for health monitor. *Sensors and Actuators B: Chemical, 209*, 281–286. https://doi.org/10.1016/j.snb.2014.11.120.

Erkan, N. (2007). Sensory, chemical, and microbiological attributes of sea bream (sparus aurata): Effect of washing and ice storage. *International Journal of Food Properties, 10*(3), 421–434. https://doi.org/10.1080/10942910600848915.

Ezati, P., Bang, Y.-J., & Rhim, J.-W. (2021). Preparation of a shikonin-based pH-sensitive color indicator for monitoring the freshness of fish and pork. *Food Chemistry, 337*, 127995. https://doi.org/10.1016/j.foodchem.2020.127995.

Ezati, P., Tajik, H., & Moradi, M. (2019). Fabrication and characterization of alizarin colorimetric indicator based on cellulose-chitosan to monitor the freshness of minced beef. *Sensors and Actuators B: Chemical, 285*, 519–528. https://doi.org/10.1016/j.snb.2019.01.089.

Fan, L., Wang, Y., Xie, P., Zhang, L., Li, Y., & Zhou, J. (2019). Copigmentation effects of phenolics on color enhancement and stability of blackberry wine residue anthocyanins: Chromaticity, kinetics and structural simulation. *Food Chemistry, 275*, 299–308. https://doi.org/10.1016/j.foodchem.2018.09.103.

Gao, T., Tian, Y., Zhu, Z., & Sun, D.-W. (2020). Modelling, responses and applications of time-temperature indicators (TTIs) in monitoring fresh food quality. *Trends in Food Science & Technology, 99*, 311–322. https://doi.org/10.1016/j.tifs.2020.02.019.

Jakobek, L., Šeruga, M., Šeruga, B., Novak, I., & Medvidović-Kosanović, M. (2009). Phenolic compound composition and antioxidant activity of fruits of Rubus and Prunus species from Croatia. *International Journal of Food Science & Technology, 44*(4), 860–868. https://doi.org/10.1111/j.1365-2621.2009.01920.x.

Jhuang, J.-R., Lin, S.-B., Chen, L.-C., Lou, S.-N., Chen, S.-H., & Chen, H.-H. (2020). Development of immobilized laccase-based time temperature indicator by electrospinning zein fiber. *Food Packaging and Shelf Life, 23*, 100436. https://doi.org/10.1016/j.fpsl.2019.100436.

Kato, N., Kunimoto, M., Koseki, S., Kitakami, S., & Arai, K.-i. (2009). Freshness and quality of fish and shellfish (Supplementary Edition). Journal of The School of Marine Science and Technology -Tokai University (Japan), 7(2), 87–99.

Khodanazary, A. (2019). Freshness assessment of shrimp *Metapenaeus affinis* by quality index method and estimation of its shelf life. *International Journal of Food Properties, 22*(1), 309–319. https://doi.org/10.1080/10942912.2019.1580719.

Kim, E., Choi, D. Y., Kim, H. C., Kim, K., & Lee, S. J. (2013). Calibrations between the variables of microbial TTI response and ground pork qualities. *Meat Science, 95*(2), 362–367. https://doi.org/10.1016/j.meatsci.2013.04.050.

Kuntzler, S. G., Costa, J. A. V., Brizio, A. P. D. R., & Morais, M. G. d. (2020). Development of a colorimetric pH indicator using nanofibers containing Spirulina sp. LEB 18. Food Chemistry, 328, 126768. 10.1016/j.foodchem.2020.126768.

Lee, H. K., Jeong, E. H., Baek, C. K., & Youk, J. H. (2005). One-step preparation of ultrafine poly(acrylonitrile) fibers containing silver nanoparticles. *Materials Letters, 59*(23), 2977–2980. https://doi.org/10.1016/j.matlet.2005.05.005.

Mataragas, M., Bikouli, V. C., Korre, M., Sterioti, A., & Skandamis, P. N. (2019). Development of a microbial Time Temperature Indicator for monitoring the shelf life of meat. *Innovative Food Science & Emerging Technologies, 52*, 89–99. https://doi.org/10.1016/j.ifset.2018.11.003.

Mokrzycki, W. S., & Tatol, M. (2011). Colour difference ΔE - A survey. Machine Graphics and Vision, 20(4), 383-411. https://www.scopus.com/inward/record.uri?eid=2-s2.0-84887450120&partnerID=40&md5=e545af56699257f98e01dc9170a506ef.

Moradi, M., Tajik, H., Almasi, H., Forough, M., & Ezati, P. (2019). A novel pH-sensing indicator based on bacterial cellulose nanofibers and black carrot anthocyanins for monitoring fish freshness. *Carbohydrate Polymers, 222*, 115030. https://doi.org/10.1016/j.carbpol.2019.115030.

Mustapha, N., Khairuddin, N., Muhamad, I., Hashim, S., & Siddique, B. (2016). Characterization of HEC/PANI film as a potential electroactive packaging with pH Sensor. *Sains Malaysiana, 45*(7), 1169–1176.

Pastoriza-Santos, I., & Liz-Marzán, L. M. (2000). Binary cooperative complementary nanoscale interfacial materials. Reduction of silver nanoparticles in DMF. Formation of monolayers and stable colloids. *Pure and Applied Chemistry, 72*(1–2), 83–90. https://doi.org/10.1351/pac200072010083.

Pinela, J., Prieto, M. A., Pereira, E., Jabeur, I., Barreiro, M. F., Barros, L., et al. (2019). Optimization of heat- and ultrasound-assisted extraction of anthocyanins from *Hibiscus sabdariffa* calyces for natural food colorants. *Food Chemistry, 275*, 309–321. https://doi.org/10.1016/j.foodchem.2018.09.118.

Pourjavaher, S., Almasi, H., Meshkini, S., Pirsa, S., & Parandi, E. (2017). Development of a colorimetric pH indicator based on bacterial cellulose nanofibers and red cabbage (Brassica oleraceae) extract. *Carbohydrate Polymers, 156*, 193–201. https://doi.org/10.1016/j.carbpol.2016.09.027.

Qin, Y., Liu, Y., Yuan, L., Yong, H., & Liu, J. (2019). Preparation and characterization of antioxidant, antimicrobial and pH-sensitive films based on chitosan, silver nanoparticles and purple corn extract. *Food Hydrocolloids, 96*, 102–111. https://doi.org/10.1016/j.foodhyd.2019.05.017.

Rahman, M. M., Bui, M. V., Shibata, M., Nakazawa, N., Rithu, M. N. A., Yamashita, H., et al. (2021). Rapid noninvasive monitoring of freshness variation in frozen shrimp using multidimensional fluorescence imaging coupled with chemometrics. *Talanta, 224*, 121871. https://doi.org/10.1016/j.talanta.2020.121871.

Shameli, K., Ahmad, M. B., Zamanian, A., Sangpour, P., Shabanzadeh, P., Abdollahi, Y., et al. (2012). Green biosynthesis of silver nanoparticles using *Curcuma longa* tuber powder. *International Journal of Nanomedicine, 7*, 5603. https://doi.org/10.2147/IJN.S36786.

Shamshad, S. I., Kher-Un-Nisa, Riaz, M., Zuberi, R., & Qadri, R. B. (1990). Shelf life of shrimp (Penaeus merguiensis) stored at different temperatures. *Journal of Food Science, 55*(5), 1201–1205. https://doi.org/10.1111/j.1365-2621.1990.tb03898.x.

Silva, C. K.da., Mastrantonio, D. J.da. S., Costa, J. A. V., & Morais, M. G.de. (2019). Innovative pH sensors developed from ultrafine fibers containing açaí (Euterpe oleracea) extract. *Food Chemistry, 294*, 397–404. https://doi.org/10.1016/j.foodchem.2019.05.059.

Su, F., Xue, J., Yang, X., Deng, H., Meng, Y., & Guo, Y. (2017). Effects of phenolic acids on copigmentation and stability of anthocyanins in red-fleshed apple. *Scientia Agricultura Sinica, 50*(4), 732–742.

Vankar, P. S., & Shukla, D. (2011). Natural dyeing with anthocyanins from Hibiscus rosa sinensis flowers. *Journal of Applied Polymer Science, 122*(5), 3361–3368.

Wan Norhana, M. N., Poole, S. E., Deeth, H. C., & Dykes, G. A. (2010). The effects of temperature, chlorine and acids on the survival of Listeria and Salmonella strains associated with uncooked shrimp carapace and cooked shrimp flesh. *Food Microbiology, 27*(2), 250–256. https://doi.org/10.1016/j.fm.2009.10.008.

Weston, M., Phan, M. A. T., Arcot, J., & Chandrawati, R. (2020). Anthocyanin-based sensors derived from food waste as an active use-by date indicator for milk. *Food Chemistry, 326*, 127017. https://doi.org/10.1016/j.foodchem.2020.127017.

Wu, X., Cui, L., Huang, B., Fu, Q., & Jin, Y. (2016). Effect of enzymatically modified isoquercitrin on the photostability of capsanthin. *Journal of Food Safety and Quality, 7*(8), 3161–3165.

Yuan, Y., & Lee, T. R. (2013). Contact angle and wetting properties. In G. Bracco, & B. Holst (Eds.), *Surface science techniques* (vol. 51, pp. 3–34). Berlin, Heidelberg: Springer. https://doi.org/10.1007/978-3-642-34243-1_1.

Zabala, S., Castán, J., & Martínez, C. (2015). Development of a time–temperature indicator (TTI) label by rotary printing technologies. *Food Control, 50*, 57–64. https://doi.org/10.1016/j.foodcont.2014.08.007.

Zhang, C., Yuan, X., Wu, L., Han, Y., & Sheng, J. (2005). Study on morphology of electrospun poly(vinyl alcohol) mats. *European Polymer Journal, 41*(3), 423–432. https://doi.org/10.1016/j.eurpolymj.2004.10.027.